

Breast Imaging

Michael A. Jacobs, PhD
 Peter B. Barker, DPhil
 David A. Bluemke, MD, PhD
 Cindy Maranto, RT
 Cheryl Arnold, RT
 Edward H. Herskovits, MD,
 PhD
 Zaver Bhujwala, PhD

Index terms:

Breast neoplasms, MR, 00.12141
 Cancer screening
 Computers, diagnostic aid
 Magnetic resonance (MR), tissue
 characterization

Published online

10.1148/radiol.2291020333
Radiology 2003; 229:225–232

Abbreviations:

IAD = intraset euclidean distance
 IED = interset euclidean distance
 ISODATA = iterative self-organizing
 data
 ROC = receiver operating characteristic

¹ From the Russell H. Morgan Department of Radiology and Radiological Science, Johns Hopkins University School of Medicine, Traylor Bldg, Room 217, 712 Rutland Ave, Baltimore, MD 21205 (M.A.J., P.B.B., D.A.B., C.M., C.A., E.H.H., Z.B.); and F. M. Kirby Research Center for Functional Brain Imaging, Kennedy Krieger Institute, Baltimore, Md (P.B.B.). Received March 22, 2002; revision requested June 11; final revision received January 13, 2003; accepted February 24. M.A.J. supported by NIH T32 CA09630 and by Breast Cancer Spore P50 CA88843. P.B.B. supported by NIH R21CA/RR91798. D.A.B. supported by NIH RFA CA96012. **Address correspondence to** M.A.J. (e-mail: mikej@mri.jhu.edu).

Author contributions:

Guarantors of integrity of entire study, M.A.J., Z.B.; study concepts, M.A.J., D.A.B., Z.B.; study design, M.A.J., D.A.B., P.B.B., Z.B.; literature research, M.A.J., D.A.B.; clinical studies, M.A.J., D.A.B., C.A., C.M.; data acquisition, C.A., C.M., M.A.J.; data analysis/interpretation, M.A.J., D.A.B., P.B.B., Z.B.; statistical analysis, M.A.J., E.H.H.; manuscript preparation, M.A.J., P.B.B., D.A.B., Z.B.; manuscript definition of intellectual content, M.A.J., Z.B.; manuscript editing, M.A.J., P.B.B., D.A.B., Z.B.; manuscript revision/review and final version approval, all authors

© RSNA, 2003

Benign and Malignant Breast Lesions: Diagnosis with Multiparametric MR Imaging¹

PURPOSE: To both develop and use a tissue signature method for the identification and classification of breast lesions and healthy breast tissue with magnetic resonance (MR) imaging.

MATERIALS AND METHODS: Thirty-six patients underwent breast MR imaging (T1- and T2-weighted imaging and three-dimensional T1-weighted imaging with and without contrast material enhancement), followed by biopsy or mastectomy and histopathologic analysis. Tissue cluster analysis was performed by using the iterative self-organizing data technique to identify glandular, adipose, and lesion tissue signature vectors. Glandular and lesion tissue vectors were characterized by angular separation from the reference adipose tissue vector. Differences in angular separation of histologically proved benign and malignant lesion groups were evaluated with an independent *t* test. The usefulness of the angular separation model for distinguishing benign from malignant lesions was evaluated with nonparametric receiver operating characteristic curve analysis.

RESULTS: The model enabled successful identification and characterization of breast lesion tissue clusters in all patients; 18 lesions were benign, and 18 were malignant. Angular separation \pm SD was $17.8^\circ \pm 6.1^\circ$ between adipose tissue and malignant lesions and $29.0^\circ \pm 11.2^\circ$ between adipose tissue and benign lesions. Angular separations of benign lesions and malignant lesions were significantly different ($P = .002$), with a specificity of 78% and sensitivity of 89% at a cutoff value of 21° . Significant differences in angular separation from adipose tissue also were found between glandular tissue and lesion tissue ($P < .001$) and, in glandular tissue, between patients with benign lesions and those with malignant lesions ($P = .04$). The area under the receiver operating characteristic curve was 0.84.

CONCLUSION: Multispectral analysis of conventional breast MR images based on the iterative self-organizing data model and on measurement of angular separation between tissue signature vectors may enable automated lesion identification and classification.

© RSNA, 2003

Magnetic resonance (MR) imaging is increasingly used for the diagnosis and characterization of suspected breast lesions identified with mammography. Contrast material-enhanced MR imaging has high sensitivity (approximately 90%) but lower specificity (approximately 37%–86%) for breast cancer detection (1–7) because certain benign lesions exhibit static or dynamic enhancement characteristics similar to those seen in breast cancers (8). For example, fibroadenomas may enhance at variable rates from slow to fast (9–14), considerably overlapping the enhancement rates of malignant lesions such as ductal carcinoma.

Attempts to increase the specificity of breast MR imaging by using computer-aided diagnosis, or CAD, have been reported previously. The methods used have included statistical measurement based on semiautomated segmentation (15–17), analysis of contrast material uptake and washout curves (5,18,19), normalized slope measurements of contrast material uptake (4), and neural network analysis (20) of contrast enhancement curves. In addition, a model comprising contrast-enhanced three-dimensional imaging

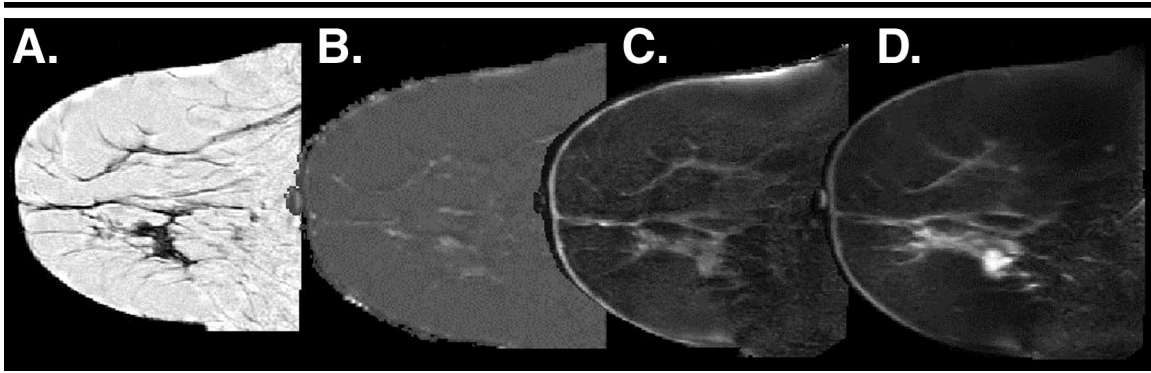


Figure 1. Representative sagittal MR image data set analyzed with the ISODATA algorithm. *A*, T1-weighted image acquired with a fast spoiled gradient-echo pulse sequence (200/4.4). *B*, Fat-suppressed T2-weighted image acquired with a spin-echo pulse sequence (5,700/102). *C*, Three-dimensional fat-suppressed T1-weighted image acquired with a fast spoiled gradient-echo pulse sequence (20/4) prior to contrast enhancement by gadodiamide. *D*, Contrast-enhanced three-dimensional T1-weighted image acquired with the same pulse sequence as in *C*.

and pharmacokinetic analysis was validated in experimental breast tumors (21) and clinical subjects (14). These methods have demonstrated specificities ranging from 39% to 83%.

The purpose of our study was to both develop and use a tissue signature method for the identification and classification of breast lesions and healthy breast tissue. We hypothesized that quantitative measurements of multiple MR signal intensities, when combined in a multiparametric model, would enable automated differentiation between different tissue types, such as adipose, glandular, and lesion tissues in the breast.

MATERIALS AND METHODS

ISODATA Model

The multiparametric MR image data set that was analyzed with the iterative self-organizing data (ISODATA) technique (22,23) consisted of T1-weighted images, fat-suppressed T2-weighted images, and three-dimensional fat-suppressed T1-weighted images acquired before and during contrast material enhancement (see MR Imaging) (Fig 1). These imaging sequences constitute the conventional breast MR imaging examination, and they were selected for ISODATA analysis because each sequence provides different contrast to disclose different tissue types. For example, T1-weighted images provide a clear visual separation of adipose tissue from glandular tissue, and T2-weighted fat-suppressed images facilitate the identification of fluid-filled structures such as cysts. Three-dimensional fat-suppressed T1-weighted images obtained prior to and during contrast enhancement help identify potential malignancies on the basis of

different enhancement caused by different uptake of the contrast agent (9,24).

If we assume that each tissue type has a characteristic signal intensity on each MR image type, then each tissue type will form a cluster in a feature space the axes of which represent the signal intensity of that tissue on MR images of that type. The center of each cluster can be described by a tissue signature vector \vec{S} , calculated for the average signal intensity of all pixels that are identified as part of the tissue type, such that $\vec{S} = S_1, S_2, \dots, S_k$, where S_k is the mean signal intensity of the tissue type on the k th image. The initial selection of normal tissue signature vectors from the MR images used in the ISODATA model is shown in Figure 2, A. The ISODATA technique (22) is an unsupervised segmentation method related to the K-means algorithm, with additional splitting and merging steps that allow for the adjustment of cluster centers. Features of the ISODATA method include the ability to adjust the number of clusters and the lack of a need for initial training or for a priori knowledge of the exact number of tissue types before segmentation. The modified ISODATA algorithm that we used consisted of four main stages, summarized as follows (for a more complete description of the 14 steps performed, see Jacobs et al [23]).

1. The criteria defining normal breast tissue parameters—in other words, adipose and glandular tissue signature vectors—and the initialization of the number of clusters were input into the program. We first defined an adipose tissue signature vector that represented the adipose tissue depicted on the MR images; a glandular tissue signature vector was likewise defined (Fig 2, A). The intraset euclidean distance (IAD) and interset

euclidean distance (IED) \pm SD for each tissue type were then computed by using ISODATA, information that was used for the splitting and merging of the different clusters. In this study, the number of initial clusters was used to partition the feature space into different segments within which tissue cluster centers would be determined. By postulating a large number of initial clusters, we ensured that all possible combinations would be accounted for. The expected number of clusters was five: adipose tissue, glandular tissue, ducts, and benign and malignant masses. We therefore set the number of initial clusters at 30—approximately an order of magnitude greater than the expected number of clusters or tissue types (ie, five).

2. The MR image feature space was partitioned into random clusters.

3. Cluster centers were determined, and IAD and IED were calculated between pixel vectors and cluster centers. IED was defined as the distance between cluster centers and was calculated from the magnitude of the difference between the two tissue cluster centers, such that $IED_{ij} = \|S_j - S_i\|$, where S_j and S_i are the cluster centers. IAD was defined as the variance of each tissue cluster, such that

$$IAD_j = \frac{1}{N_j} \sum_{i=1}^{N_j} \|S_i^j - S_j\|,$$

where N_j is the number of pixels in the j th cluster, S_i^j is the i th data point in the j th group, and S_j is the cluster center.

4. The clusters were then split and merged on the basis of the projected IAD and IED. The splitting and merging of clusters allowed for adjustment to the number of clusters on the basis of the structure of the data.

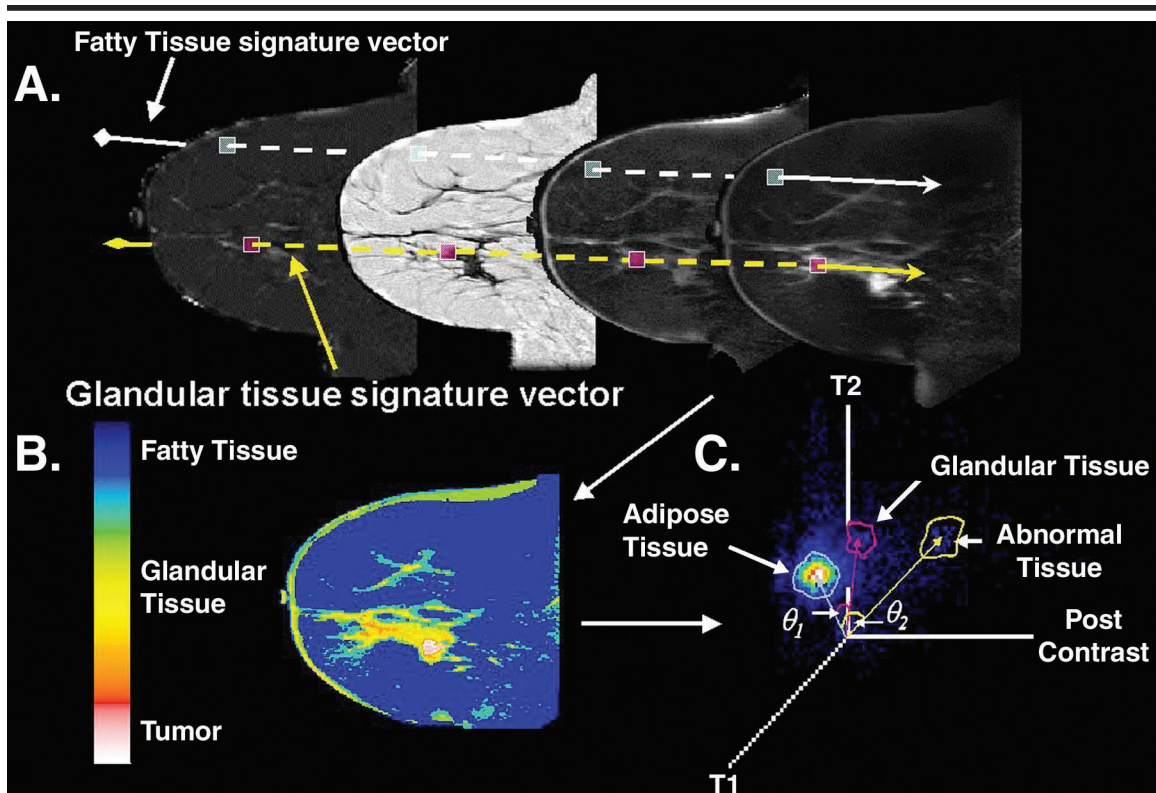


Figure 2. MR image data from the same patient as in Figure 1. *A*, Diagram of signature vectors defined for each normal tissue type (adipose and glandular) and assigned to the tissue cluster that most closely resembles the vector elements for that tissue type in the ISODATA algorithm. *B*, Representative ISODATA theme map of the signature vectors defined for each tissue cluster shows normal adipose tissue (dark blue) in most of the breast. Regions that are light blue, green, and yellow represent glandular tissue, and pink and white areas represent tumor tissue. *C*, Diagram of the three-dimensional feature space formed by the combination of T1-weighted images and T2-weighted fat-suppressed images with contrast-enhanced three-dimensional images. The angular separation model, with the distribution of tissue clusters in the three-dimensional feature space, is shown. Angles were calculated as the dot product between the normal tissue cluster and the abnormal tissue cluster by using each cluster's tissue signature vector (θ_1 , θ_2). Each axis represents the signal intensity distribution for each MR image type.

Steps 3 and 4 were repeated until the data converged (ie, the SD of the clusters was minimized) or the maximum number of iterations was reached (Fig 2, *B*).

Study Subjects

A total of 36 patients (age range, 18–80 years; median, 45 years) were included in this study. The protocol was approved by the Joint Committee on Clinical Investigation at the Johns Hopkins University School of Medicine, and informed consent was obtained from all subjects.

Subjects were selected retrospectively from a cohort of 60 patients who were referred consecutively over the course of 1 year (from February 2000 to March 2001) for MR evaluation of suspected breast lesions identified at mammography, ultrasonography, and/or clinical examination. MR images of 11 patients could not be evaluated with the ISODATA method because of technical difficulties such as improper field of view ($n = 6$), inadequate fat

suppression ($n = 3$), archival problems ($n = 1$), and failure of image coregistration ($n = 1$). From the remaining 49 patients whose images were technically adequate, the research coordinator (C.M.), who was not blinded to histologic findings, selected at random 18 patients who had received a diagnosis of benign breast lesion and 18 patients who had received a diagnosis of carcinoma. This study design was based on statistical considerations (ie, the need to have equal numbers of patients in each group). The cases were presented in random order to the MR imaging physicist (M.A.J.), who performed image analysis while blinded to histologic findings. After MR imaging, core or excisional biopsies were performed in 20 patients, and the other 16 patients underwent lumpectomy or mastectomy.

Histologic Analysis of Lesions

After MR imaging, biopsies were performed on lesions identified on mammo-

grams and MR images and at physical examination. Tissue specimens from mastectomy were cooled to approximately 5°C. Specimens were sliced at 5–10-mm intervals, in the same plane in which the MR images were acquired.

Each lesion was classified as benign or malignant on the basis of histologic analysis. A lesion was considered benign if the histologic report specified fibrocystic changes, including formation of cysts or increased fibrous tissue, with benign patterns of ductal or lobular distortion and benign cellular changes such as are seen in typical or atypical lobular or ductal hyperplasia. A lesion was considered malignant if it was diagnosed histologically as ductal, lobular, or undifferentiated carcinoma.

MR Imaging

For mammographically identified lesions, the mammogram and mammographic report were made available to the radiologist (D.A.B.) for correlation with

TABLE 1
Patient Age, Lesion Size, and MR Imaging and Histologic Findings in Patients with Benign Lesions

Patient No.	Patient Age (y)	Lesion Size (cm)	MR Finding*	Histologic Finding
1	63	1.2	Positive	Benign fibrous breast tissue with microcalcifications
2	41	4.8	Positive	Benign breast tissue with fat necrosis
3	45	1.6	Positive	Apocrine metaplasia and cystic dilatation
4	46	2.0	Positive	Fibroadenoma
5	74	2.0	Positive	Residual atypical ductal hyperplasia, apocrine metaplasia, and intraductal papilloma
6	44	4.0	Positive	Fibrocystic change
7	46	2.2	Positive	Stromal fibrosis and elastosis. Florid ductal epithelial hyperplasia and sclerosing adenosis
8	38	2.0	Positive	Fibroadenoma
9	48	1.8	Positive	Fibroadenoma
10	46	3.6	Positive	Fibrocystic change and adenosis
11	53	1.0	Positive	Benign breast tissue with fibrocystic change
12	42	0.9	Positive	Benign breast tissue with fibrocystic change, ductal hyperplasia, and adenosis with microcalcifications
13	45	0.5	Positive	Benign breast tissue
14	41	2.5	Positive	Markedly atypical ductal hyperplasia with microcalcifications
15	32	3.5	Positive	Benign breast tissue with fibrocystic change
16	44	1.0	Positive	Benign breast tissue with fibrocystic change
17	44	1.2	Positive	Ductal ectasia and intense inflammatory infiltrate
18	59	1.2	Positive	Benign breast tissue with fibrocystic change and microcalcifications
Mean	47.3	2.1		
SD	9.7	1.2		

* Positive indicates that contrast enhancement was observed in the lesion on MR images acquired after administration of gadodiamide.

MR images. For abnormalities identified at physical examination, a marker was placed on the breast prior to MR imaging.

MR imaging was performed with a 1.5-T MR imager (GE Medical Systems, Waukesha, Wis) and a dedicated phased-array breast coil (MRI Devices, Milwaukee, Wis), with the patient lying prone and the breast in the holder to reduce motion. The imaging protocol included a fat-suppressed T2-weighted spin-echo pulse sequence (repetition time msec/echo time msec, 5,700/102) and a T1-weighted fast spoiled gradient-echo sequence (200/4.4) with a field of view of 18 × 18 cm, matrix of 256 × 192, section thickness of 4 mm, and 1-mm gap between sections. In addition, a three-dimensional fat-suppressed T1-weighted fast spoiled gradient-echo pulse sequence (20/4, image matrix of 512 × 160, section thickness of 2 mm) was performed before and during contrast enhancement obtained with intravenous administration of 0.2 mL/kg (0.1 mmol/kg) gadodiamide (Omniscan; Amersham Health, Princeton, NJ). The contrast agent was hand injected over a period of 10 seconds, followed by a 20-mL normal saline solution flush, with MR imaging beginning immediately after completion of the injection. Total imaging time for the entire protocol was less than 20 minutes.

MR Image Preprocessing and Analysis

MR image preprocessing and analysis were performed at a workstation (Ultra-

SPARC60; Sun Microsystems, Mountain View, Calif). Images were preprocessed with image analysis software (Eigentool; Image Analysis Lab, Henry Ford Hospital, Detroit, Mich) (25–28). Subimaging of the breast from the background was achieved by using thresholding and morphologic operations (29) to reduce computational time. After subimaging, an inhomogeneity correction method was applied to the MR image data set (30). Finally, the images were restored by using a nonlinear restoration filter to reduce image noise while preserving edges and partial volume effects (31). To account for possible patient motion, misalignment between sequences, and differences in section location or thickness, coregistration of the breast MR images was accomplished by a method described previously (30).

Quantitative MR Measurements

Tissue clusters were defined by using multiparametric ISODATA segmentation and identified according to tissue signature vector (32). Tissue signature vectors were defined for the adipose and glandular tissues in each patient (Fig 2, A) and were used as input values for the ISODATA algorithm. Other tissue types were automatically determined by the ISODATA routine, which output a theme map with different colors representing the different tissue types (Fig 2, B). Adipose tissue depicted on the theme map produced by multiparametric ISODATA

segmentation was visually verified by a radiologist (D.A.B.) according to its appearance on T1- and T2-weighted images. The adipose tissue vector defined by ISODATA segmentation was used as the reference vector for measurement of angular separation of the other tissue clusters defined by ISODATA and depicted on the theme map. Classification of the different tissue types was determined on the basis of angular separation between the two tissue signature vectors (Fig 2, C), which was calculated by using the dot product between the vectors. The results obtained with the ISODATA model for each lesion were compared with the histopathologic findings.

To identify the combination of MR data that would provide optimal visual separation of breast tissue types in feature space, ratios of IED to IAD were calculated between pixel vectors and cluster centers from the different MR image data sets. Whereas IED is the distance between each tissue cluster center, and IAD is the variance within each tissue cluster, the ratio of IED to IAD is a measure of separation (33,34) between the different tissue clusters in feature space. The four MR image data sets considered for optimal separation were (a) T1- and T2-weighted images; (b) T1- and T2-weighted images and fat-suppressed (nonenhanced) T2-weighted images; (c) T1- and T2-weighted images and three-dimensional fat-suppressed contrast-enhanced T1-weighted

TABLE 2
Patient Age, Lesion Size, and MR Imaging and Histologic Findings in Patients with Malignant Lesions

Patient No.	Patient Age (y)	Tumor Size (cm)	MR Finding*	Histologic Finding
1	46	1.0	Positive	Infiltrating mammary carcinoma with one focus of ductal carcinoma
2	52	1.3	Positive	Infiltrating well-differentiated ductal carcinoma with atypical ductal hyperplasia
3	56	1.1	Positive	Infiltrating ductal carcinoma and benign fibroadipose tissue
4	80	1.0	Positive	Infiltrating mammary carcinoma with ductal and lobular features
5	50	1.0	Positive	In situ ductal carcinoma with microcalcifications
6	54	2.5	Positive	Invasive poorly differentiated mammary carcinoma with associated focal ductal carcinoma in situ
7	47	1.0	Positive	In situ ductal and infiltrating poorly differentiated ductal carcinoma with microcalcifications
8	58	1.4	Positive	Infiltrating lobular carcinoma, lobular carcinoma in situ, and foci of ductal carcinoma
9	40	2.5	Positive	Ductal carcinoma, solid and cribriform types
10	60	2.2	Positive	Infiltrating ductal carcinoma
11	62	2.0	Positive	Infiltrating ductal carcinoma
12	34	5.0	Positive	Carcinoma
13	62	6.0	Positive	Differentiated ductal carcinoma
14	70	3.6	Positive	Infiltrating ductal carcinoma
15	63	1.0	Positive	Infiltrating ductal carcinoma with mucinous features
16	52	1.3	Positive	In situ and infiltrating mammary carcinoma
17	34	3.0	Positive	In situ carcinoma
18	59	2.6	Positive	Infiltrating ductal carcinoma
Mean	54.4	2.2		
SD	11.8	1.5		

* Positive indicates that contrast enhancement was observed in the lesion on MR images acquired after administration of gadodiamide.

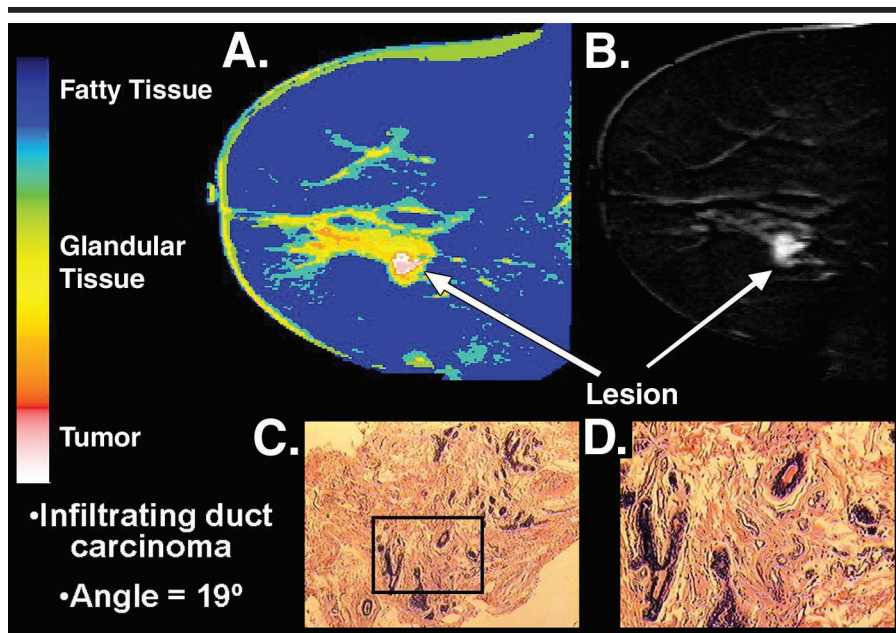


Figure 3. MR image data from a 56-year-old woman with infiltrating ductal carcinoma confirmed by histologic analysis following mastectomy. *A*, Theme map obtained with multiparametric ISODATA segmentation at an angular separation threshold of 19° demonstrates clear delineation of adipose tissue (blue) from glandular tissue (light green to yellow). *B*, Sagittal T1-weighted contrast-enhanced digital subtraction image acquired with a FSPGR pulse sequence (20/4). *C*, *D*, Histologic photomicrographs (hematoxylin-eosin stain, original magnification in *C*, $\times 2$; in *D*, $\times 40$) on which the tumor tissue appears in pink and white. The histologic morphology of the lesion was consistent with that of infiltrating ductal carcinoma.

images; and (d) T1- and T2-weighted images and three-dimensional fat-suppressed contrast-enhanced and nonenhanced T1-weighted images.

Statistical Analysis

Differences in angular separation between benign and malignant lesion groups

were evaluated by using an independent Student *t* test. Statistically significant difference was considered to be indicated by $P < .05$. In addition, the ability of the angular separation model to discriminate between benign lesions and malignant lesions was evaluated with nonparametric receiver operating characteristic (ROC) curve analysis.

RESULTS

The histopathologic and MR imaging findings for the patient population in this study are shown in Tables 1 and 2. On gadolinium-enhanced T1-weighted images, all of the breast lesions were contrast enhanced; contrast enhancement was the criterion used to define a lesion.

The multiparametric ISODATA model enabled successful segmentation of normal and abnormal breast tissues and differentiation between adipose and glandular tissue types in all cases. Figure 3 shows a representative multiparametric ISODATA segmentation from a 56-year-old patient with infiltrating ductal carcinoma confirmed at histologic analysis after mastectomy. The ISODATA segmentation of adipose and glandular tissues is shown in Figure 3, *A*. Representative histologic photomicrographs of tissue from the lesion area are shown in Figure 3, *C* and *D*. The angular separation of tumor tissue from adipose tissue was 19.6°, whereas the separation of glandular tissue from adipose tissue was 7.1°. Overall,

TABLE 3
Angular Separations of Glandular Tissue and of Lesion Tissue from the Adipose Tissue Reference, Calculated for Malignant and Benign Lesions

Lesion	Angular Separation of Glandular Tissue from Adipose Tissue (degrees)		Angular Separation of Lesion Tissue from Adipose Tissue (degrees)	
	Mean	SD	Mean	SD
Malignant (<i>n</i> = 18)	5.6*	2.4	17.8†	6.1
Benign (<i>n</i> = 18)	7.8	3.5	29.0	11.2

* *P* = .04 indicates a significant difference between malignant and benign lesions.

† *P* < .002 indicates a significant difference between malignant and benign lesions.

for malignant lesions (*n* = 18), the average angular separation between adipose tissue and tumor tissue was $17.8^\circ \pm 6.1^\circ$ (mean \pm SD). For benign lesions (*n* = 18), the average angular separation between adipose tissue and lesion tissue was $29.0^\circ \pm 11.2^\circ$.

Angular separation of lesion tissue from adipose tissue was significantly different between benign and malignant lesions (*P* < .002, *df* = 26, *t* statistic = -3.64). Angular separation from adipose tissue also was significantly different between glandular tissue and lesion tissue (*P* < .001, *df* = 22, *t* statistic = -7.41). In addition, there was a significant difference in glandular tissue signature vectors between patients with benign lesions and those with malignant lesions (*P* = .04, *df* = 30, *t* statistic = 2.04) (Table 3). Figure 4 shows the ROC curve used to evaluate the ability of the ISODATA-based angular separation model to differentiate benign lesions from malignant lesions. The area under the ROC curve is 0.84. The sensitivity and specificity of several representative angular separation thresholds are presented in Table 4.

The MR data set that included T1-weighted and T2-weighted images and contrast-enhanced and nonenhanced three-dimensional T1-weighted images had the largest IED/IAD ratio—2.54 for the lesion tissue cluster and 1.51 for the glandular tissue cluster (Table 5). This result indicates that this image data set provided the best separation in feature space. The large IED/IAD ratio also suggests that this data set may be optimal for achieving increased separation between tissue types and decreased variance within each tissue type. Two data sets (T1- and T2-weighted images combined with contrast-enhanced three-dimensional T1-weighted images, and T1- and T2-weighted images combined with non-enhanced three-dimensional T1-weighted images) had similar IED/IAD ratios for the lesion tissue cluster (1.85 and 1.80, respec-

tively) and glandular tissue cluster (1.31 and 1.32, respectively). The T1- and T2-weighted image data set exhibited the lowest IED/IAD ratio for the lesion tissue (ie, 1.68) and glandular tissue types (ie, 1.19).

DISCUSSION

The results of this study indicate that a quantitative, multiparametric approach to breast MR imaging may enable the automated characterization of breast lesions as benign or malignant. The application of the angular separation model to MR image analysis provides quantitative information that may assist the radiologist in determining whether a lesion is benign or malignant. Further evaluation will be necessary to determine whether this quantitative assessment improves the accuracy of clinical diagnosis of breast cancer.

Other investigators previously reported that T1- and T2-weighted images are not sufficient for distinguishing benign from malignant tissue (1,10,35) and that contrast-enhanced MR image data allow for better visualization of the tumor extent and of multifocality in breast masses suspected to be malignant (4,9). The results of our study indicate that quantitative analysis of all MR data is useful for tissue classification as benign versus malignant. Although T1- and T2-weighted images alone may not be useful for differentiating tissue types, the combination of these images with contrast-enhanced three-dimensional T1-weighted images increases the distance between tissue clusters and minimizes the spread of values within a single cluster. This assertion is supported by the IED/IAD ratios calculated for the different image data sets; the multiparametric data set consistently provided a higher IED/IAD ratio than the other data sets.

T1-weighted images can provide excellent visual separation of adipose tissue from glandular tissue, and T2-weighted

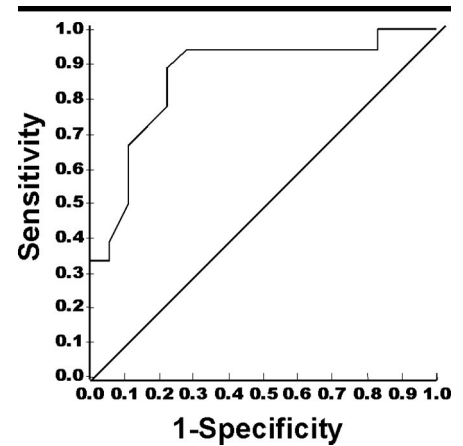


Figure 4. Graph of ROC curves for ISODATA-based analysis of angular separation according to lesion tissue type and for all tissues. The area under the curve for lesion tissue type was 0.84. The diagonal line indicates an area under the curve of 0.50 (ie, no separation between tissue types).

TABLE 4
Sensitivity and Specificity of the Model at Six Threshold Angle Values for Prediction of Benign versus Malignant Lesions

Threshold Angle (degrees)	Sensitivity (%)	Specificity (%)
17	33	94
18	50	89
19	67	89
21	89	78
22	94	72
23	94	67

images can depict cysts, necrosis, hemorrhage, and some fibroadenomas (1,10,35). Previous investigators, such as Kuhl et al (35), suggested that the incorporation of T2 weighting and contrast material enhancement into the breast MR imaging protocol could increase diagnostic specificity. Most malignant breast lesions are profoundly enhanced after administration of a contrast agent, and the enhancement pattern may aid in the differential diagnosis of the lesion (5,18). However, some benign lesions, such as fibroadenomas, tend to enhance to the same extent as carcinomas. To overcome this difficulty, Degani et al (21) used the contrast enhancement patterns on MR images obtained at three different time points during contrast material uptake to produce a color-coded theme map that characterized tumor heterogeneity in terms of microvascular permeability and extracellular fraction. The use of this three-time-point imaging and mapping method was shown to improve the accu-

TABLE 5
Comparison of IED/IAD Ratios among the Four Image Data Sets Studied, for Glandular and Lesion Tissue Clusters

MR Image Data Set	IED/IAD Ratio for Tissue Cluster	
	Glandular Tissue	Lesion Tissue
T1- and T2-weighted images	1.19	1.68
T1- and T2-weighted images and fat-suppressed (nonenhanced) T2-weighted images	1.32	1.80
T1- and T2-weighted images and three-dimensional fat-suppressed contrast-enhanced T1-weighted images	1.31	1.85
T1- and T2-weighted images and three-dimensional fat-suppressed contrast-enhanced and nonenhanced T1-weighted images	1.51	2.54

racy of diagnosis of fibroadenoma (14). This area of breast imaging has been reviewed recently (36).

In our study, malignant lesions had smaller angular separations from adipose tissue than did benign lesions, but the mechanisms underlying these differences in angular separation have yet to be determined. MR imaging is highly sensitive both to localized changes in tissue water content and to changes in the general environment produced by the exchange of water with the surrounding tissue. Changes in tissue water content can reflect physiologic and morphologic alterations that occur during the growth of tumors. The use of extracellular gadolinium-based contrast agents improves the detection of most malignant breast lesions by means of observed lesion vascularity, architecture, and permeability. The timing of the contrast material injection and of breast imaging influences the signal intensity on MR images.

Malignant breast lesions tend to exhibit a washout pattern on dynamic contrast-enhanced images that differs from that of benign lesions, which usually exhibit either persistent or plateau-type enhancement (5). However, benign lesions and malignant lesions can have the same contrast enhancement pattern (5,14). The time delay between contrast material injection and image acquisition may influence the angular separation between the lesion tissue and adipose tissue, resulting in the smaller angle seen in malignant lesions; this hypothesis requires further evaluation in future studies.

Of the four MR image data sets used in our ISODATA segmentation model, the multiparametric set that included all four types of MR images consistently produced better tissue cluster separation as defined by the IED/IAD ratio than the other MR data sets. In the sets lacking contrast-enhanced image data, the lesion

was not optimally segmented from the surrounding tissues. The T1- and T2-weighted image data set had the lowest IED/IAD ratio. Our study results indicate that the inclusion of contrast-enhanced three-dimensional T1-weighted images allowed for better segmentation of the breast tissue.

Breast tumors, whether benign or malignant, tend to have longer T1 and T2 relaxation times than does normal breast tissue (37,38). Malignant tumors have shorter T1 and T2 relaxation times than do benign lesions, although there may be some overlap in relaxation times between the two lesion groups (37,38). This difference in relaxation times may be related to increased water content in benign lesions and may have produced the increased angular separation observed in this study.

The results of previously published studies indicate that MR imaging has high sensitivity but lower specificity for the detection of breast lesions. In most of these studies, time-intensity curves were used to measure the dynamic enhancement of signal intensity over time, after injection of a contrast agent. Some investigators, using time-intensity curves alone, have demonstrated a sensitivity of approximately 91% for lesion detection with MR imaging, with specificities ranging from 37% to 86% (5,39–43).

Adams et al (15) evaluated the combined use of T1- and T2-weighted images with intermediate-weighted and Dixon-opposed breast MR images and supervised segmentation classifiers in a three-dimensional feature space. Supervised segmentation requires a training data set to teach classifiers how to recognize different tissue types. In addition, Adams et al evaluated shape analysis, in which compactness and frequency of lesion boundary characteristics are considered. They found shape analysis important for

separating benign from malignant tumors on the basis of T1-weighted, T2-weighted, and Dixon-opposed MR images. Lucas-Quesada et al (16) constructed a two-dimensional feature space from contrast-enhanced and nonenhanced MR images and employed two semiautomated methods for segmentation of breast tumors. The two methods gave similar segmentation results, with accuracy of 76%–84% (according to the authors' criterion); however, the segmented lesions were not classified as benign or malignant.

Gilhuijs et al (17) reported the use of a model for computer-aided diagnosis based on the extraction of different features from dynamic contrast-enhanced images, including the uptake of contrast material, sharpness of lesion definition, shape of the lesion, and radial gradient. Features were evaluated individually and in combination by means of ROC analysis. The combination of radial gradient with sharpness gave the best results (ROC area, 0.86–0.87 for two-dimensional analysis and 0.92–0.96 for three-dimensional analysis), with specificity of 77% and sensitivity of 100%. Lucht et al (20), using a neural network classifier and time-intensity curves derived from breast MR images, achieved a sensitivity of 84% and specificity of 81%.

To our knowledge, our study is the first evaluation of a four-dimensional multiparametric MR image data set consisting of T1- and T2-weighted images and contrast-enhanced and nonenhanced three-dimensional T1-weighted images. The results achieved with our classification method are comparable to those of other, similar studies. For example, with an angular separation of 21°, sensitivity of 89% and specificity of 78% were achieved. At larger angles, sensitivity of 94% and specificity of 72% were realized. These data demonstrate the potential of the angular separation model for correctly identifying and classifying breast lesions. The advantage of the model described in this article is that it may be adapted to include five dimensions (eg, dynamic contrast enhancement) or more (eg, shape analysis [44], diffusion coefficients, or sodium imaging [45]). The goal of subsequent multiparametric analysis will be to determine the minimum number of parameters that objectively and quantitatively yield optimal sensitivity and specificity.

In conclusion, multispectral analysis of conventional MR images by means of ISODATA and measurements of angular separation may provide an automated means of breast lesion identification and

classification. This approach may enable the identification of specific tissue signatures characteristic of benign versus malignant breast lesions.

Acknowledgments: We gratefully acknowledge Donald Peck, PhD, Physics and Engineering Division head, Hamid Soltanian-Zadeh, PhD, senior staff scientist, and Lucie Bower, BS, systems analyst at the Image Analysis Lab, Henry Ford Health System, Detroit, Mich, for providing the Eigentool image analysis software used in image processing, and the anonymous reviewers of the manuscript for their constructive comments.

References

- Heywang SH, Bassermann R, Fenzl G, et al. MRI of the breast: histopathologic correlation. *Eur J Radiol* 1987; 7:175-182.
- Gilles R, Guinebretiere JM, Shapeero LG, et al. Assessment of breast cancer recurrence with contrast-enhanced subtraction MR imaging: preliminary results in 26 patients. *Radiology* 1993; 188:473-478.
- Fischer U, Kopka L, Brinck U, Korabiowska M, Schauer A, Grabbe E. Prognostic value of contrast-enhanced MR mammography in patients with breast cancer. *Eur Radiol* 1997; 7:1002-1005.
- Kelcz F, Santyr GE, Cron GO, Mongin SJ. Application of a quantitative model to differentiate benign from malignant breast lesions detected by dynamic, gadolinium-enhanced MRI. *J Magn Reson Imaging* 1996; 6:743-752.
- Kuhl CK, Mielcarek P, Klaschik S, et al. Dynamic breast MR imaging: are signal intensity time course data useful for differential diagnosis of enhancing lesions? *Radiology* 1999; 211:101-110.
- Orel SG. High-resolution MR imaging for the detection, diagnosis, and staging of breast cancer. *RadioGraphics* 1998; 18:903-912.
- Kuhl CK. MRI of breast tumors. *Eur Radiol* 2000; 10:46-58.
- Weinreb JC, Newstead G. MR imaging of the breast. *Radiology* 1995; 196:593-610.
- Heywang SH, Hahn D, Schmidt H, et al. MR imaging of the breast using gadolinium-DTPA. *J Comput Assist Tomogr* 1986; 10:199-204.
- Kerslake RW, Carleton PJ, Fox JN, et al. Dynamic gradient-echo and fat-suppressed spin-echo contrast-enhanced MRI of the breast. *Clin Radiol* 1995; 50:440-454.
- Heywang-Kobrunner SH, Haustein J, Pohl C, et al. Contrast-enhanced MR imaging of the breast: comparison of two different doses of gadopentetate dimeglumine. *Radiology* 1994; 191:639-646.
- Gribbestad IS, Nilsen G, Fjosne HE, Kvinnsland S, Haugen OA, Rinck PA. Comparative signal intensity measurements in dynamic gadolinium-enhanced MR mammography. *J Magn Reson Imaging* 1994; 4:477-480.
- Orel SG, Schnall MD, LiVolsi VA, Troupin RH. Suspicious breast lesions: MR imaging with radiologic-pathologic correlation. *Radiology* 1994; 190:485-493.
- Weinstein D, Strano S, Cohen P, Fields S, Gomori JM, Degani H. Breast fibroadenoma: mapping of pathophysiological features with three-time-point, contrast-enhanced MR imaging—pilot study. *Radiology* 1999; 210:233-240.
- Adams AH, Brookeman JR, Merickel MB. Breast lesion discrimination using statistical analysis and shape measures on magnetic resonance imagery. *Comput Med Imaging Graph* 1991; 15:339-349.
- Lucas-Quesada FA, Sinha U, Sinha S. Segmentation strategies for breast tumors from dynamic MR images. *J Magn Reson Imaging* 1996; 6:753-763.
- Gilhuijs KGA, Giger ML, Bick U. Computerized analysis of breast lesions in three dimensions using dynamic magnetic-resonance imaging. *Med Phys* 1998; 25:1647-1654.
- Orel SG. Differentiating benign from malignant enhancing lesions identified at MR imaging of the breast: are time-signal intensity curves an accurate predictor? *Radiology* 1999; 211:5-7.
- Sinha S, Lucas-Quesada FA, DeBruhl ND, et al. Multifeature analysis of Gd-enhanced MR images of breast lesions. *J Magn Reson Imaging* 1997; 7:1016-1026.
- Lucht RE, Knopp MV, Brix G. Classification of signal-time curves from dynamic MR mammography by neural networks. *Magn Reson Imaging* 2001; 19:51-57.
- Degani H, Gusic V, Weinstein D, Fields S, Strano S. Mapping pathophysiological features of breast tumors by MRI at high spatial resolution. *Nat Med* 1997; 3:780-782.
- Ball G, Hall D. ISODATA, a novel method of data analysis and pattern classification. Technical Report no. 4. Menlo Park, Calif: Stanford Research Institute, April 1965.
- Jacobs MA, Knight RA, Soltanian-Zadeh H, et al. Unsupervised segmentation of multiparameter MRI in experimental cerebral ischemia with comparison to T2, diffusion, and ADC MRI parameters and histopathological validation. *J Magn Reson Imaging* 2000; 11:425-437.
- Kacl GM, Liu P, Debatin JF, Garzoli E, Caduff RF, Krestin GP. Detection of breast cancer with conventional mammography and contrast-enhanced MR imaging. *Eur Radiol* 1998; 8:194-200.
- Jacobs MA, Knight RA, Windham JP, et al. Identification of cerebral ischemic lesions in rat using eigenimage filtered magnetic resonance imaging. *Brain Res* 1999; 837:83-94.
- Peck D, Windham J, Emery L, Soltanian-Zadeh H, Hearshen D, Mikkelsen T. Cerebral tumor volume calculations using planimetric and eigenimage analysis. *Med Phys* 1996; 23:2035-2042.
- Soltanian-Zadeh H, Windham J, Peck D, Yagle A. A comparative analysis of several transformations for enhancement and segmentation of magnetic resonance image scene sequence. *IEEE Trans Med Imaging* 1992; 11:302-318.
- Windham JP, Abd-Allah MA, Reimann DA, Froelich JW, Hagggar AM. Eigenimage filtering in MR imaging. *J Comput Assist Tomogr* 1988; 12:1-9.
- Soltanian-Zadeh H, Windham JP. A multiresolution approach for contour extraction from brain images. *Med Phys* 1997; 24:1844-1853.
- Jacobs MA, Windham J, Soltanian-Zadeh H, Peck D, Knight R. Registration and warping of magnetic resonance images to histological sections. *Med Phys* 1999; 26:1568-1578.
- Soltanian-Zadeh H, Windham JP, Yagle AE. A multidimensional nonlinear edge-preserving filter for magnetic resonance image restoration. *IEEE Trans Image Processing* 1995; 4:147-161.
- Jacobs MA, Bluemke DB, Bhujwala Z, Marano C, Barker PB. A model to differentiate benign from malignant breast tumors using multiparametric MRI with histological correlates (abstr). In: Proceedings of the ninth meeting of the International Society for Magnetic Resonance in Medicine. Berkeley, Calif: International Society for Magnetic Resonance in Medicine, 2001; 563.
- Tou J, Gonzales R. Pattern recognition principles. Reading, Mass: Addison-Wesley, 1974.
- Theodoridis S, Koutroumbas K. Pattern recognition. Vol 1. San Diego, Calif: Academic Press, 1999.
- Kuhl CK, Klaschik S, Mielcarek P, Gieseke J, Wardelmann E, Schild HH. Do T2-weighted pulse sequences help with the differential diagnosis of enhancing lesions in dynamic breast MRI? *J Magn Reson Imaging* 1999; 9:187-196.
- Orel SG, Schnall MD. MR imaging of the breast for the detection, diagnosis, and staging of breast cancer. *Radiology* 2001; 220:13-30.
- Merchant TE, Thelissen GR, de Graaf PW, Nieuwenhuizen CW, Kievit HC, Den Otter W. Application of a mixed imaging sequence for MR imaging characterization of human breast disease. *Acta Radiol* 1993; 34:356-361.
- McSweeney MB, Small WC, Cerny V, Sewell W, Powell RW, Goldstein JH. Magnetic resonance imaging in the diagnosis of breast disease: use of transverse relaxation times. *Radiology* 1984; 153:741-744.
- Boetes C, Barentsz JO, Mus RD, et al. MR characterization of suspicious breast lesions with a gadolinium-enhanced TurboFLASH subtraction technique. *Radiology* 1994; 193:777-781.
- Gilles R, Guinebretiere JM, Lucidarme O, et al. Nonpalpable breast tumors: diagnosis with contrast-enhanced subtraction dynamic MR imaging. *Radiology* 1994; 191:625-631.
- Harms SE, Flamig DP, Hesley KL, et al. MR imaging of the breast with rotating delivery of excitation off-resonance: clinical experience with pathological correlation. *Radiology* 1993; 187:493-501.
- Heiberg EV, Perman WH, Herrmann VM, Janney CG. Dynamic sequential 3D gadolinium-enhanced MRI of the whole breast. *Magn Reson Imaging* 1996; 14:337-348.
- Daniel BL, Yen YF, Glover GH, et al. Breast disease: dynamic spiral MR imaging. *Radiology* 1998; 209:499-509.
- Nunes LW, Schnall MD, Orel SG. Update of breast MR imaging architectural interpretation model. *Radiology* 2001; 219:484-494.
- Ouwerkerk R, Jacobs MA, Bottomley PA, Fajardo LL. A method for quantifying tissue sodium in breast tumors with short echo time 23Na MRI (abstr). In: Proceedings of the tenth meeting of the International Society for Magnetic Resonance in Medicine. Berkeley, Calif: International Society for Magnetic Resonance in Medicine, 2002; 2060.